Gasa *et al. Journal of Electric Propulsion* (2025) 4:70
https://doi.org/10.1007/s44205-025-00169-3

Journal of Electric Propulsion

RESEARCH Open Access

Experimental characterization of a low current thermionic dry neutralizer in an electron gun configuration for ion engines

Klevis Gasa[1*], Zuzanna Nagadowska[2], Alexander Daykin-Iliopoulos[1,2], Francesco Guarducci[2] and Stephen B. Gabriel[1,2]

*Correspondence:
Klevis Gasa
kg2n21@soton.ac.uk
[1]Tony Davies High Voltage Laboratory, University of Southampton, Southampton, UK
[2]Mars Space Ltd, Southampton, UK

Abstract

A critical aspect of the development of next-generation electric propulsion systems for new deep-space small satellites and CubeSats is the neutralization system. Dry, or propellantless, neutralizers represent an attractive alternative to the conventional wet neutralization systems as a cathode current < 100 mA can be achieved with a low power input (< 20 W) with significant specific impulse savings, propellant system simplification and potential power savings. Using a validated 2D axisymmetric COMSOL Multiphysics model, a thermionic dry neutralizer based on an electron gun configuration has been designed, developed, and experimentally characterized. The experimental characterization in diode mode has investigated the influence on the cathode emission and system losses of the extraction electrode voltage and anode voltage respectively in the 100–580 V and 0–30 V range. Experimental results show good agreement with simulation predictions used in the design phase. The electric field focusing and space charge de-focusing effects to minimize power losses are discussed. Furthermore, the thermal influence of the emitter temperature is explored from 1110 ° C to 1200 ° C assessing the minimum operational power, poisoning effects, and thermal hysteresis. The neutralizer has achieved a maximum anode current of 55.8 mA at an extraction electrode biasing voltage < 600 V and a heater power consumption of 10.5 W, resulting in a total power-to-current ratio of 0.32 W/mA. Thus, technologically demonstrating emission and power characteristics suitable for thruster neutralization of small satellites and CubeSat applications.

Keywords Dry neutralizer, Propellant-less neutralizer, Thermionic cathode, Electron gun, Low current

Introduction

The increasing interest in small-scale satellites as economic, efficient, and versatile systems for space applications relies on the development of next-generation propulsion systems [1, 2]. Upcoming missions such as the Next-Generation Gravity Mission (NGGM) [3] and the Miniaturized Asteroid Remote Geophysical Observer (M-ARGO) can be enabled via small electric propulsion technologies for orbit correction, drag

compensation, and de-orbiting [4, 5]. Such missions require high delta-V and high total impulse but low power and thrust levels, and this can be achieved by miniaturized gridded ion engines such as the RIT3.5 [6–8] or the MiXI [9, 10]. One of the critical aspects to be evaluated, due to the limited power budget and space availability, is the neutralization system. The charge balance of the exhausted plume is a critical operational requirement for any electric propulsion device since non-neutralization could cause a failure of the electric propulsion system or the systems on board. For small low-power thrusters such as the RIT3.5, the currents needed for the neutralization are typically in the 0-100 mA range [11], depending on the thrust setpoint and number of engines.

Various neutralization technologies developed for low current neutralization are summarized in Table 1. For low-current operations, hollow cathodes (HC) require a high flow rate relative to the main thruster flow and additional power to the cathode to sustain the self-heating process, with a consequent reduction of the specific impulse associated with the required flow and mass efficiency reduction due to the feeding system [9, 12–14]. Because of the reduction in the heat fluxes to the emitter resulting from the low discharge current, an additional heater and/or keeper current is usually required [14–16]. Several developed HCs have demonstrated operation capability at discharge currents < 0.3 A with this additional power [9, 17–20]. To reduce the required heat fluxes, novel emitter materials such as calcium aluminate electride, C12A7, are under research. Being able to operate at temperatures well under 1000 °C, experimental testing reports discharge currents in the 0.1–0.3 A range [21, 22]. However, the C12A7 is unable to support long operativity due to poor emission uniformity, discharge voltage instabilities, and lifetime issues. Detailed reviews of the hollow cathodes for low current application and the challenges involved in this application are provided in Reference [12, 16]. Field emitter arrays (FEA) offer an attractive solution for small low-power electric propulsion missions since they do not require heating power and a propellant flow [1, 12]. Several FEAs have been developed and tested for demonstrating the ability to emit up to 1 mA [23–25]. Higher currents could be achieved by increasing the number of arrays and their size, as the 88 mm x 88 mm neutralizer capable of emitting 20 mA [25]. However, for 100 mA emission a 390 cm^2 footprint would be required, which is very challenging for small satellite applications. Filament neutralizers could provide enough electron current in the 0-100 mA with low power consumption, however, their limited lifetime with respect to the other neutralization technologies due to life-limiting mechanisms such as material evaporation at high temperature and ion bombardment, limits their application [15, 26]. Dry dispenser cathodes, i.e., thermionic cathodes operating without the need for a gas flow, have been investigated [15, 27, 28] and adopted for space applications in configurations able to produce 1–10 mA [29–32]. Without self-heating as with hollow cathodes, dispenser cathodes used as dry neutralizers (DN) require continuous heater power. An extraction electrode biased with respect to the cathode extracts the electrons from the thermionic emitter in a space-charge limited condition. An example is the neutralizer unit adopted for the Lisa Pathfinder's thruster shown in Table 1 as FEEP NU [30]. An emitted cathode current of 20 mA is reached with 200 V on the extraction gate electrode bias voltage; however, nearly half of the emitted current is lost to the extraction gate electrode, resulting in a reduction in power efficiency [29]. This effect is caused by the space-charge effect on the electron beam, and it can be mitigated by introducing a second electrode, typically referred to as the focusing electrode. This approach is widely

Table 1 Neutralizers developed for low current operation and their characteristics

Name	Institution	Type	Current [mA]	Max Bias Voltage [V]	Flow [sccm]	Emitter Type	Operational Power [W]	Power to Current Ratio [W/mA]	Current to Surface Ratio [mA/ cm^2]	Lifetime	Thruster	Ref.
MiXI Cathode	UCLA	HC	15–200	-	0.03-1	BaO–W	15 W start-up, 13–20 W operation	0.07–1.3	-	-	MiXI	[9]
SHC-0.3 A	Kharkiv Aviation Institute	HC	200–1000	-	0.5	BaO–W	30 W start-up, 4–7.5 W operation	0.02	15,000–25,000 A/ cm^2	17,000 h	SPT-20 M	[17, 39]
ARC-1 A	Rafael	HC	200–1200	-	1.01–2.54	BaO–W	25–55 W	0.02–0.1	-	5000 h endurance test	CAM200	[19, 40]
HC1	SITAEL	HC	300–1000	-	0.8-5	LaB_6	50 W start-up, 9–20 W operation	0.013–0.023	-	>10,000 h	HT100	[20]
NRL Cathode	Naval Research Laboratory	HC	30–150	-	5–30	C12A7	30 W start-up, 21–27 W operation	0.14–0.19	20–40	16 h	-	[22]
Busek Cathode	Busek Co.	FEA	0.01-1	250–800	-	CNT	0.4	0.4	0.8	6000 h endurance test at 1 mA	Busek mN Colloid	[23, 41]
TUD Cathode	TU Dresden	FEA	0.25	400	-	CNT	0.4	1.6	0.4	500 h endurance test	NanoFEEP	[24, 42]
FE cathode	JAXA	FEA	3–20	500	-	CNT	1–6	0.3	0.26	-	30 W ion engine	[25]
FEEP NU	Thales Alenia Space	DN	6–10	200	-	BaO–W	5	0.5–0.9	110	3500 h endurance test	FEEP micro-Thruster	[29, 43]
Enpulsion Cathode	Enpulsion	DN	3–5	200	-	Ta	4	0.8	-	>10,000 h	IFM FEEP Nano Thruster	[31, 44, 45]

Note: Omitted data is either not available or not applicable

adopted for dispenser cathodes in an electron gun configuration on magnetrons, traveling wave tubes, and cathode-ray tubes [33]. This electrode is set at cathode potential, and it is used to focus the beam by reducing radial electric field components to counter the coulomb repulsion between electrons in the beam [33, 34], increasing the magnitude of the extracted electron beam as the gate electrode collects less current. A dedicated electron gun configuration could allow it to operate at higher voltages and consequently increase the emission current up to 100 mA with low power consumption and reduced complexity. However, when integrated with ion thrusters, electron gun-based neutralizers may face coupling limitations due to their operating method. Unlike hollow cathodes, which operates by creating a plasma bridge that draw out the cathode's electrons through a potential difference to the thruster beam, electron guns operate under space-charge limited condition as they emit a focused electron beam rather than generating a plasma. As a result, the interaction between the electron beam and the ion plume can be less efficient, potentially leading to incomplete or unstable charge neutralization, spacecraft charging, or beam divergence issues. This could be addressed by reducing the distance between the neutralizer and the ion source, making it easier for the electrons to reach the ion beam. However, having the dry neutralizer too close to the ion beam could increase the risk of ion sputtering that can degrade critical components like the emitter surface and reduce the device's operational lifetime. That said, the emitter itself is expected to be protected by the highly positive bias applied to the extraction electrode, which repels incoming ions and minimizes direct bombardment.

This work presents the design and characterization of a low-current dry neutralizer that would enable neutralization of the beam current required by low-power thrusters, such as the RIT3.5 [8, 11, 13]. Due to the application requirements to operate with a low voltage on the extraction electrode [13], a high perveance electron gun configuration is required, i.e., $P > 1$ μPerv [34]. This type of configuration has a large extraction aperture that strongly perturbs the electric field. Validated analytical models can be found in the literature for the design of electron guns [35]. However, for high-perveance devices, numerical methods are essential due to the complexity of the fields and the particle behaviour [34]. Thus, a 2D-axisymmetric electron optics model based on an electron gun configuration has been developed on COMSOL [36]. Based on the initial simulation results, a breadboard setup was designed and experimentally tested to validate the model. Additional experiments were conducted by varying electrode distances and orifice sizes to gain further insight into the emission characteristics and to compare them with model predictions. Following this iterative validation process, a refined electron optics configuration was defined. This study presents the test results of this final breadboard configuration, referred to as the Dry Neutralizer 3.4 (DN3.4), where "3.4" indicates the emitter diameter in millimetres. The neutralizer was tested in diode mode with an anode plate collecting the emitted electron current under conditions representative of operation with an ion thruster. The influence of the extraction electrode voltage and the anode voltage were investigated to characterise the neutraliser's performance. The DN3.4 has also been successfully operated in coupled mode with the RIT3.5, demonstrating stable performance up to 2.5 mN, corresponding to 35.5 mA of emission, as reported in Ref [37, 38]. A comparison between the diode and coupled mode test will be reported in a future work.

The first section of this work describes the breadboard design and setup. The second section aims to describe the test facility, the instrumentations, and the test procedures. The third section presents the results of the thermal characterization and the operational experimental characterization, demonstrating higher emission current with an enhanced power efficiency than has been previously achieved for such applications. In the final section, conclusions are drawn on the capability of the DN3.4 to generate sufficient electron emission current to represent a viable neutralizer solution for ion thrusters.

Neutralizer design

The DN3.4 is a modular breadboard configuration composed of two units, namely the firing unit and the emitter unit. The two units are connected on the two opposite sides of a stainless-steel mounting plate, and a set of spacers allows for easy manipulation of the emitter-to-electrodes distance, as shown in Fig. 1a. A Thorlabs optical base is used for accurate positioning of the system components in the chamber. A stainless-steel anode disk with a diameter of 180 mm is placed 20 mm downstream of the DN3.4 for the diode mode testing. The anode has an orifice of 5 mm in the centre to permit the vision of the emitter surface through a chamber window and enable pyrometer measurements. Figure 1b shows a schematic drawing of the setup with a simplified representation of the main elements that compose the DN3.4. The firing unit consists of two electrode plates, the gate extraction electrode and the focusing electrode. The electrodes are kept isolated and at a fixed distance by a ceramic alumina plate, while the power and voltage sensing connections are achieved through a set of mechanical fixtures. The firing unit also includes a stainless-steel casing element to screen the gate extraction electrode. Different optics can be tested by changing the electrodes' geometry or by changing their relative positions by using spacers. The emitter unit consists of a dispenser cathode connected to a cathode support plate that allows the connection to the mounting plate. The

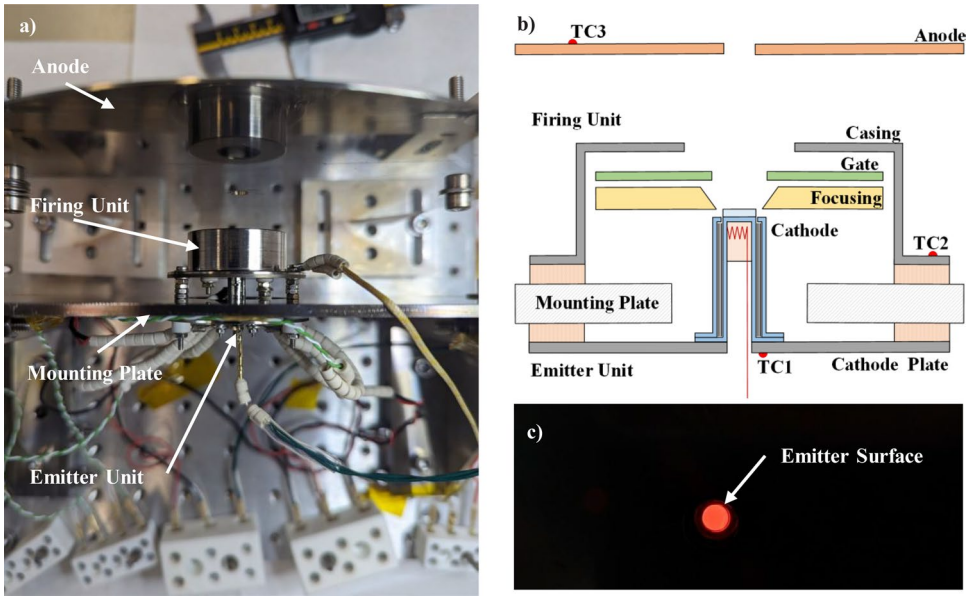

Fig. 1 DN3.4 setup mounted in MSL-VC3 chamber with the anode plate and connectors; **a**) top-view of the experimental test setup, **b**) Schematic drawing of the setup showing the firing unit and the emitter unit connected to the mounting plate and the thermocouples location, (**c**) emitter surface glow during operation seen through the anode aperture

cathode adopted for this test campaign is a cylindrical dispenser cathode with an integrated heater potted in alumina. The emitter is a disc of 3.4 mm in diameter and 1 mm in thickness of porous tungsten emitter impregnated with barium-calcium-aluminate. According to the manufacturer bulleting, the emitter should be able to produce more than 10 A/cm2 at 1200 °C with a lifetime estimated to be above 80,000 h, assuming barium depletion to be the dominant lifetime-limiting mechanism and relying on pre-existing barium depletion model [46]. Multi-layered molybdenum thermal shielding is wrapped around the cathode tube to reduce the radiative thermal losses of the DN3.4 during operation, and it is kept in position by a radiation shield casing. All connections go through block connectors to the chamber feedthrough. Type-K thermocouples are attached to the test setup to monitor the temperatures during operation. Figure 1b shows their location at the base of the cathode, TC1, at the base of the casing, TC2, and at the far end of the anode, TC3. Figure 1c shows the emitter glow visible through the anode aperture during operation.

Test methodology

Electric configuration

An overview of the electrical schemes for the experimental test campaign can be seen in Fig. 2. An EA-PS 9750-12, 750 V–12 A power supply applies a voltage bias between the gate extraction electrode and the cathode. A TTI CPX400DP-Dual Supply, 60 V–20 A-420 W, is used for the anode and the cathode. One channel is used to bias the anode plate with respect to ground, while the other sets a bias on the cathode common potential with respect to the facility ground to recreate the operating potential when coupled with a thruster. A second TTI CPX400DP-Dual Supply is used to operate the heater, while the casing was connected to facility ground. All current measurements are performed by measuring the voltage drop across $1\Omega \pm 1\%$ shunts, not shown in the schematic. The heater voltage and current are measured by two TESTEC TT – SI

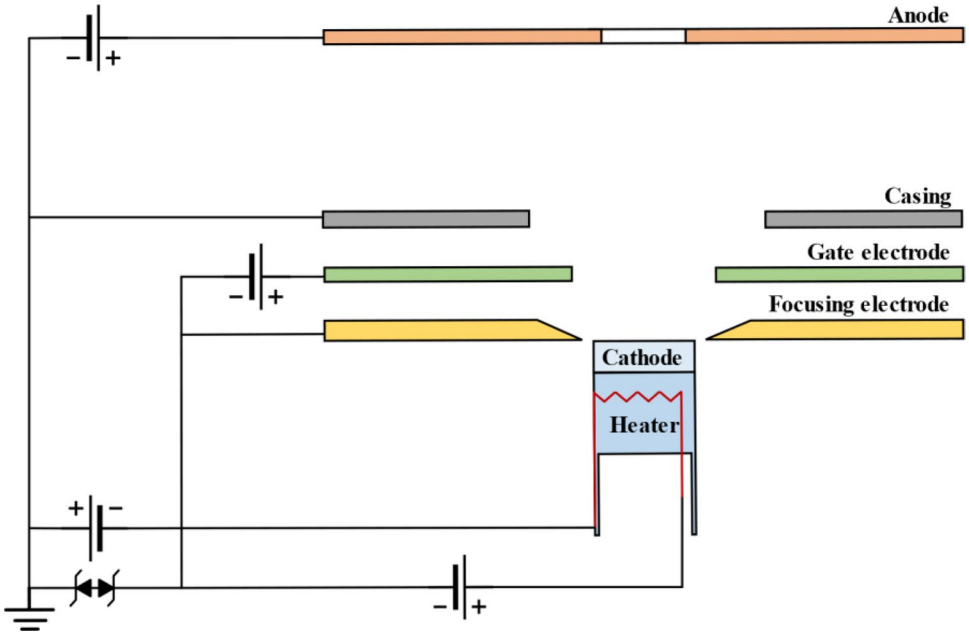

Fig. 2 Schematic of the main electric configuration

9001 differential voltage probes, that measure up to ± 70 V. With a ± 2% accuracy on the measurement, the heater power error at 10.5 W is ± 0.42 W. Both probes are connected to a Tektronix DPO3014, 100 MHz 4-channel Digital Oscilloscope, which displays and records the heater current and voltage. A Keysight 34,970 A data acquisition unit along with a 34,901 A 20-channel multiplexer module is used to conduct all the remaining voltage and thermocouples measurements. The accuracy is measured as a % of reading + % of scale range. At the highest range, 300 V, the error corresponds to 0.0035% of the reading + 0.0030% of the range, thus a maximum of 0.02 V of error. While for the currents, the scale range used was 100mV. The accuracy is 0.0040% of reading + 0.0040% of the range, resulting at most in a ± 0.007 mA for the cathode current of 77.4 mA.

Finally, a protection circuit composed of two zener diodes between the cathode common floating potential and the facility ground is introduced. This was introduced to avoid excessive variation of the floating potential that could lead to equipment damage and create unsafe testing for the personnel.

All the power supplies, the oscilloscope, the multiplexer, and the pressure gauge are connected to a PC and logged by a LabView program at a sample rate of approximately 1 Hz. All interfaces between the control system and test apparatus are isolated via inline USB/RS232 optocouplers. The software allows you to monitor, record, and control all the test setup, but also to execute automated test operations by stepping through a list of user-defined operating points loaded in configured test sequence files.

Test facility

The test campaign was performed at the MSL EP laboratory in Southampton, UK. The DN3.4 was tested in MSL-VC3, which is a stainless-steel vacuum chamber with a diameter of 490 mm and a length of 510 mm, shown in Fig. 3a. A door mounted on a frame structure to a rail system allows the chamber to open, and an ISO-K180 viewport on the side allows optical access. The chamber is equipped with a pumping system composed of a backing pump and a turbo-molecular pump that enables the chamber to reach an ultimate pressure of 8×10^{-8} mbar during the DN3.4 operation. Figure 3b shows a

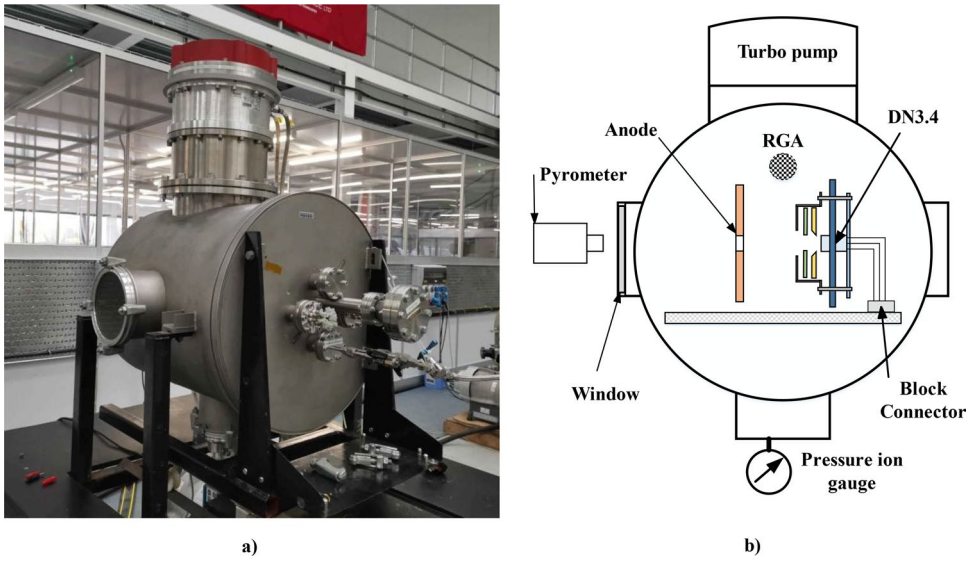

Fig. 3 **a**) MSL-VC3 vacuum chamber in the MSL EP laboratory, **b**) front-view of the MSL-VC3 vacuum facility with the DN3.4 setup configuration schematic

front-view schematic of MSL-VC3 along with the position of the different instruments adopted for the test campaign.

A Keller Mikro PV 11 optical pyrometer is used to measure the emitter surface brightness temperature. This pyrometer operates at a wavelength, λ, of 0.65 μm, and has a total range of 700 °C to 3000 °C. A tungsten filament is heated until its brightness color matches the hot body. For accurate pyrometer measurements, the brightness temperature has to be converted to the true temperature according to the following relation [47, 48]:

$$\frac{1}{\mathrm{T}} - \frac{1}{\mathrm{T}_\lambda} = \frac{\log \epsilon_\lambda \zeta}{9613} \tag{1}$$

where T is the true temperature in K, T_λ is the brightness temperature in K, λ the wavelength, $?_\lambda$ is the emissivity, while ζ is the chamber window optical transmittance at λ. For a BaO-W emitter, at 0.65 μm, the emissivity is assumed equal to 0.52 [48], while for the glass window of the chamber, the optical transmittance is taken to be 0.91 as typical for borosilicate glass [49]. A measuring uncertainty is 1.5% of the measured value in the 700–800 °C range and 0.6% of the measured value in the 800–2000 °C range. An additional uncertainty dependent on the pyrometer operator is on average 1.5 °C at 1000 °C, and 3 °C for repeatability.

A Lesker KJLC354 Series hot filament ion gauge with an integrated controller is positioned on the bottom of the chamber and it is used to monitor the total background pressure in the system. A residual gas analyzer (RGA), SRS RGA200, connected opposite to the door, is used to keep track of the partial pressures during the DN3.4 test campaign. RGA readings during nominal conditions and test operation are shown in Table 2.

Test parameters and procedures

Dispenser cathodes, such as the BaO-W emitter used in the DN3.4, require an adequate vacuum level to operate. The pressure close to the cathode has to be lower than 1.3×10^{-7} mbar, otherwise, the emitter surface would experience poisoning effects and the emission would be reduced [50]. Moreover, a commissioning phase is required whenever the cathode is operated for the first time following exposure to air and humidity [51]. The procedure adopted involves maintaining the cathode under vacuum at ~ 400 °C and then at ~ 900 °C for up to 12 h to ensure complete outgassing. This was followed by activation phase in which the cathode was operated at an emission temperature of 1200 °C until a stable cathode emission is achieved before the performance characterization

Table 2 RGA readings during DN operation compared to nominal conditions

Gas Type		Mass [amu]	Ultimate Partial Pressure [mbar]	DN in Operation	
				Average Partial Pressure [mbar]	Peak Partial Pressure [mbar]
Hydrogen	H_2	2	1.1×10^{-9}	9.3×10^{-9}	5.2×10^{-8}
Atomic Nitrogen	N	14	1.6×10^{-9}	1.7×10^{-9}	2.9×10^{-9}
Ammonia / Hydroxide	NH_3 / OH^-	17	6.1×10^{-10}	6.3×10^{-10}	1.1×10^{-9}
Water	H_2O	18	2.4×10^{-10}	2.5×10^{-9}	4.2×10^{-9}
Nitrogen	N_2	28	1.5×10^{-8}	1.6×10^{-8}	1.8×10^{-8}
Oxygen	O_2	32	3.1×10^{-9}	3.2×10^{-9}	4.8×10^{-9}
Carbon Dioxide	CO_2	44	2.1×10^{-10}	4.2×10^{-10}	5.3×10^{-9}

tests. Poisoning effects could be avoided by using lanthanum hexaboride (LaB_6) due to its greater resistance to impurities and air exposure. However, its significantly higher operating temperature results in an increase in power demand, making it less suitable for low-power systems. Moreover, since emission occurs from the bulk material, LaB_6 evaporation over time alters the surface geometry [46], leading to changes in performance due to modified electron optics.

Once the commissioning phase was completed, the DN3.4 characterization tests were performed by varying the gate electrode biasing voltage and the anode voltage. The cathode temperature during operation was preliminarily set to 1200 °C to avoid emission reduction due to poisoning effects, which depend on the emitter temperature and the operating pressure. A lower temperature of the emitter or a higher pressure in the chamber increases the poisoning [50]. For the characterization, the cathode was set at -60 V respect to ground to simulate the operation with the thruster, the gate voltage was varied in the range of 100–580 V, in increments of 100 V, while the anode voltage was set to 0 V, 10 V, and 30 V. However, the voltage readings measured by the multiplexer were consistently around 1% lower, attributed to voltage drops across the shunts. To assure steady-state conditions, every measurement was taken when the cathode was thermally and electrically stable (< 0.2 V/h and < 0.2 A/h for the heater, < 0.1 mA/h variation for all measured currents). Successively, the effects of the emitter temperature on the currents at 580 V on the gate and 30 V on the anode were investigated. The characterization was performed by sweeping the heater power, and consequently the emitter temperature, three times from 1225 °C to 1115 °C, and then increasing it back to the same level. Each setpoint was recorded once the current rate of change was lower than 0.2 mA/h or after 2 h, depending on which occurred first.

The emitted cathode current, I_c, during operation could be collected by the focusing and gate extraction electrode, expressed by I_F and I_G, or leave the gate orifice, expressed by the bias current I_B. The bias current is then collected by the anode or the casing, respectively I_A and I_{cas}. These relations are summarized in Eq. 2 and Eq. 3, and are illustrated in Fig. 4. All the currents were acquired except the casing current that was derived from Eq. 3. Thus, casing current includes potential losses through the facility.

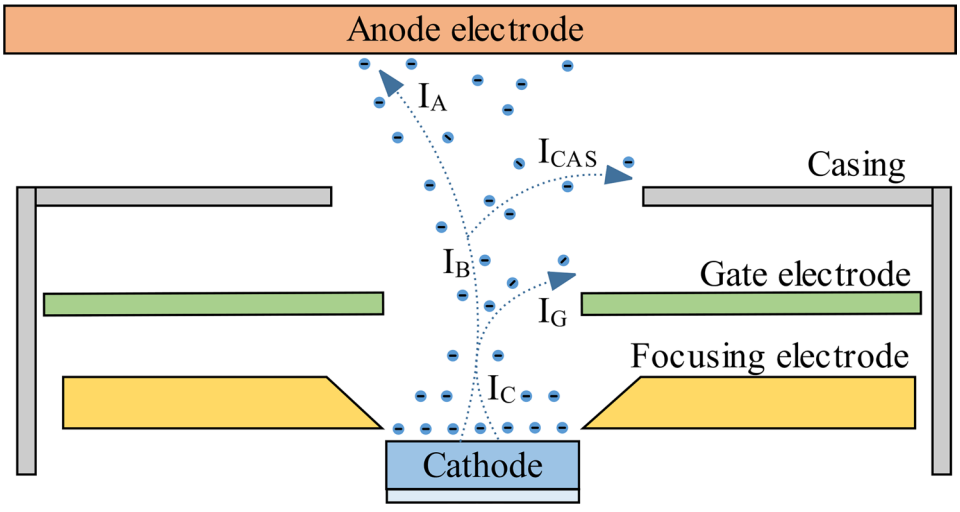

Fig. 4 Emitted cathode current distribution

$$\mathrm{I_c} = \mathrm{I_G} + \mathrm{I_B} + \mathrm{I}_F \tag{2}$$

$$\mathrm{I_B} = \mathrm{I_A} + \mathrm{I_{cas}} \tag{3}$$

Results and discussion

Thermal characterization

Thermal characterization provides an understanding of temperature distributions, which play a key role in optimizing the dry neutralizer power requirements. Figure 5a shows emitter brightness temperature profile and true temperature, derived from Eq. 1, as a function of the heater power. Error bars indicate the measuring uncertainties of the pyrometer since these exceed the standard deviation. The emitter reaches a temperature of 1200 °C with a power on the potted heater of 10.5 W, but it can operate at lower temperatures within the RIT3.5 power requirements [11]. Figure 5b shows the temperatures measured on the cathode base, the anode plate, and the casing base as a function of the emitted temperature between 1100 and 1125 °C. The data was derived from six power sweeps performed during the operation. Error bars are displayed as 3σ, to ensure the uncertainties are visible in the figure. The cathode base temperature remains below 350 °C in this range while the casing and the anode are respectively at around 150 °C and 75 °C. While the cathode base is heated due to conduction, the other two result from radiation and electron beam heating.

Gate voltage and anode voltage influence

This section focuses on the characterization of the operating voltages' influence on the emission. Six voltage sweeps at 1200 °C have been conducted, three increasing and three decreasing sweeps, and the results are presented in this section. Error bars showing standard deviation have been included to illustrate the level of repeatability of the results. Figure 6 shows the results of the gate extraction electrode voltage sweep with the anode voltage set to 30 V compared with the model predictions. There is a fairly good agreement between the model and the experimental results in terms of currents trends. The experimental cathode current is consistently higher than the one predicted by the model, which results in higher currents measured on the other electrodes. This discrepancy could be explained by the inherent difficulty in ensuring the setup configuration

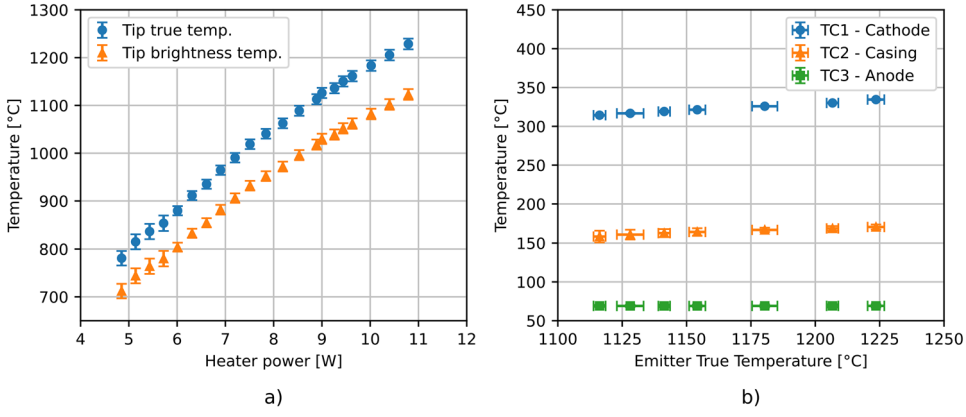

Fig. 5 Thermal profiles of the DN3.4; **a**) emitter surface brightness temperature and true temperature as a function of the heater power, **b**) temperatures at the base of the DN3.4 components as a function of the emitter true temperature during operation

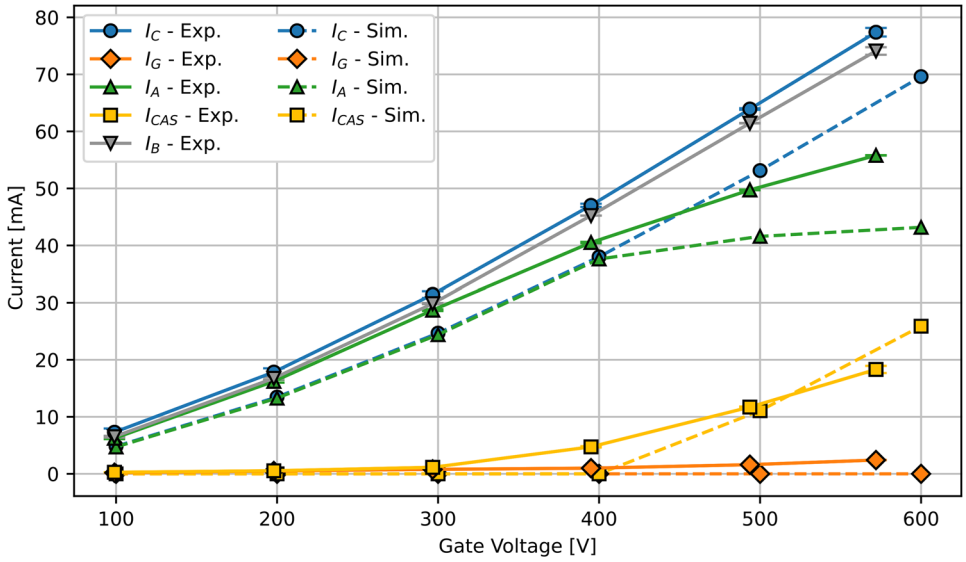

Fig. 6 Comparison between the simulation predictions and the currents measured experimentally as a function of the gate electrode voltage at 30 V on the anode

being identical to the model. A small variation in the distances between the electrodes, the thermal expansions of the different components, or the misalignments between the electrodes are sources of deviation. The model predicts no current to the gate, while in the experiments it is small but non-negligible. The anode current shows good agreement with the simulation up to approximately 400 V. Beyond this point, the experimental values deviate from the model, although both exhibit a similar increasing trend with reduced slope, corresponding to the increased current collected by the casing.

Experimentally, the cathode current varies with the gate electrode voltage from 7.1 mA at 100 V on the gate to 77.4 mA at 580 V with high repeatability. The dependence of this current on the gate voltage exhibits a non-linear trend consistent with the space-charge limited emission current regime, $I_C \propto V^{3/2}$, showing good agreement with the general profile predicted by the model. This indicates that the emission is primarily governed by space charge effects rather than cathode temperature, as the measured current remains significantly below what would be expected in the thermionic emission regime. This behaviour can be explained by the Child-Langmuir law, which defines the maximum current extractable from the cathode-to-gate region and confirms that the system operates in space-charge limited regime. Downstream the casing, electrodes retain a finite kinetic energy due to the stronger acceleration in the cathode-to gate region compared to the deceleration in the gate-to-casing region. As a result, electrons leave the casing with an energy of about 60 eV. Additionally, the outward bulging of the potential at the casing aperture [36] reduces the effectiveness of the deceleration, allowing the electrons to retain an energy of more than 100 eV at the exit of the neutraliser. Entering the casing-to-anode region with non-zero energy, the electrons are governed by the generalised Child-Langmuir law for non-zero initial velocity [52], which predicts a space-charge limited current consistent with the measured anode current.

It is observed that the focusing electrode effectively focuses the beam as the gate current is low at all voltages, being at most 2.4 mA of the total emitted cathode current. Thus, most of the current results in bias current, i.e., current that leaves the gate

electrode. Up to 300 V, the bias current is collected primarily by the anode, with a casing current that remains in the order of 1 mA. However, at higher voltages, the current collected by the casing increases at the expense of the anode current. At 580 V, the anode current corresponds to 55.8 mA, with 18.3 mA lost on the casing and facility. Higher voltages and higher bias current result in an increased divergence of the beam and a higher space-charge downstream of the casing orifice [36]. Part of the diverged electrons are then attracted and collected by the casing, resulting in a power loss to the system. This behaviour would be reduced when operated with an ion source which would decrease the downstream space-charge divergence. A focusing electrode current was detected being around 0.7 mA of current during the test activity. Because of the low dependence on the operating conditions, it is not shown in the figures.

The total power required to operate the DN3.4 is approximately 18 W, including heater power, the power lost on the electrodes of the DN and on the anode. Specifically, 10.5 W are needed to keep the emitter to its operating temperature of 1200 °C, the gate electrode collects 2.4 mA at 580 V respect to the cathode, resulting in 1.4 W, while the casing draws 18.3 mA at 60 V respect to the cathode, contributing by 1.1 W. An extra 5 W derive from considering the 55.8 mA on the anode plate at 90 V respect to the cathode. However, this power would not be included in the power budget of the DN when operated with a thruster, as there would be no dedicated anode electrode. In a coupled configuration, the ion beam from the thruster effectively acts as the anode and this power would represent a performance loss in the coupled system. By considering the anode current, 55.8 mA, as the portion of the electron current available for beam neutralization, the resulting power-to-current ratio is 0.32 W/mA and a current-to-surface ratio of 615 mA/cm^2, which compares favourably with the values in Table 1. In comparison, the FEEP NU from Table 1 can emit 6–10 mA with a power consumption of 0.5–0.9 W/mA, since half of the cathode current is collected by the gate [29, 43], while the IFM Nano Thruster's dry neutralizer has a power to current ratio of 0.8 W/mA with a total emission of 5 mA [32].

Figure 7 shows the anode voltage influence on the currents as a function of the gate voltage. The cathode current is primarily governed by the gate voltage and is nearly unaffected by the anode voltage. This indicates that the emission is determined solely by the firing unit's optics. At 580 V, the difference between the cathode current at 0 V and 30 V on the anode appears to be 2.1 mA, around 3% of the total current. A similar behaviour, minimum influence, can also be observed in the bias current and gate current. Up to 300 V, the currents seem almost independent of the anode voltage, while at higher gate voltages, the difference between the 0 V and 30 V conditions is only 1.2 mA for the gate and 3.3 mA for the bias. However, the anode voltage does influence the distribution between the gate current and bias current: higher anode voltage leads to an increase in bias current and a corresponding decrease in gate current. This again is explained by the equilibrium between the electric field forces and the electron beam self-repulsion. A higher anode voltage draws more electrons, reducing the space-charge effect and the beam divergence. In contrast, the anode voltage significantly affects both the anode current and casing current. At 580 V, the anode current at 30 V is 55.8 mA compared with 36 mA for the 0 V case. The reduction in anode current at lower voltages results in a corresponding increase in the casing current of up to 35 mA. As the anode voltage increases, the electric field near the anode becomes stronger and extends

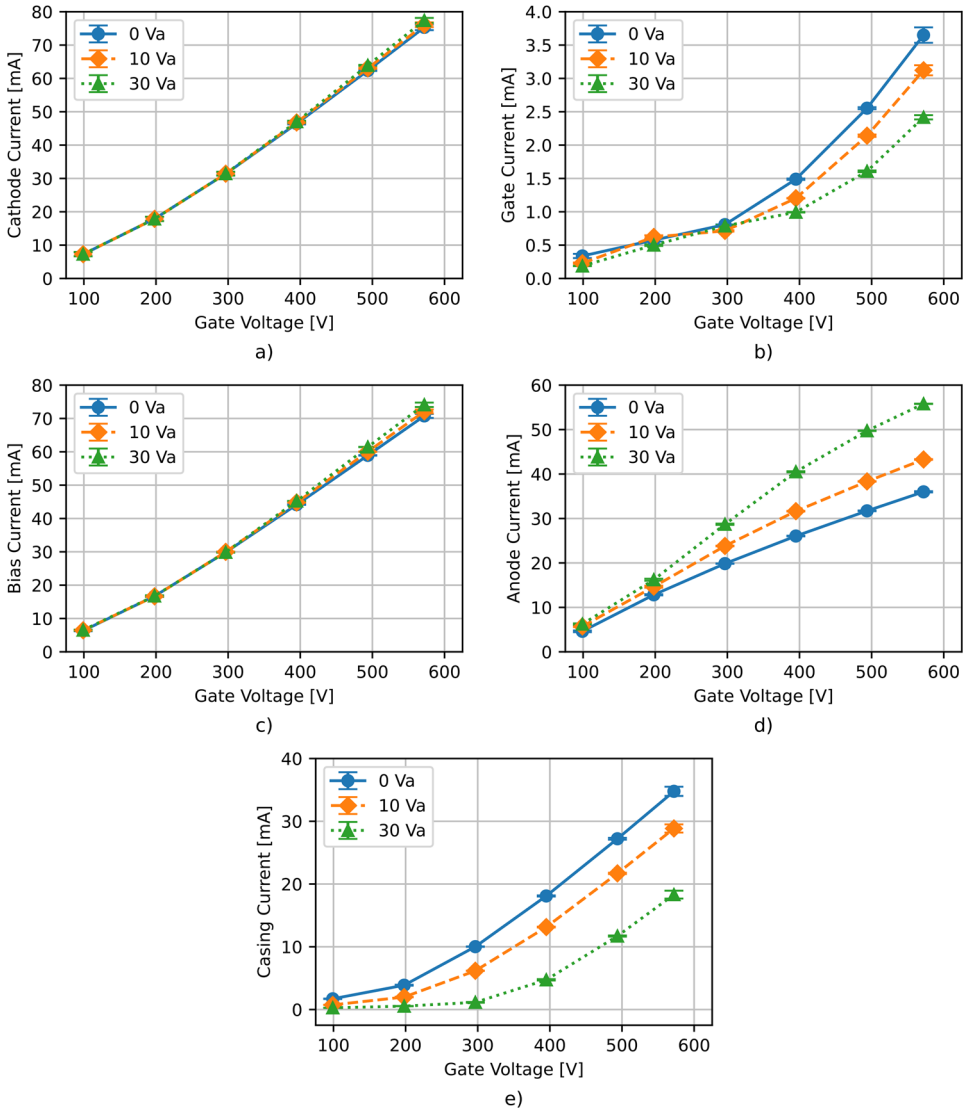

Fig. 7 Currents as a function of the gate voltage at various anode voltage; **a**) cathode current, **b**) gate current, **c**) bias current, **d**) anode current, **e**) casing current

further upstream, effectively attracting a greater portion of the emitted electron beam. This results in a more focused and directed flow of electrons toward the anode, thereby reducing the fraction of electrons intercepted casing and the gate. Consequently, both the gate and casing currents decrease with increasing anode voltage, while the anode current increases. The relatively high casing current is a result of the specific design characteristics of the system, as the breadboard was partially protruding into the electron beam due to limitations in the breadboard mounting interfaces. In the engineering model [8], the casing current is expected to decrease by minimizing the casing-to-gate distance, a result that will be confirmed through further testing.

The transmission rate of the DN is defined as the ratio of the anode current to the total emitted current, the cathode current, and gives an indication of how efficiently the anode current is extracted. Figure 8 shows the transmission rate along with the ratio of the other electrodes as a function of the gate voltage at various anode voltages. At least 94% of the emitted cathode current leaves the firing unit as bias current except for the

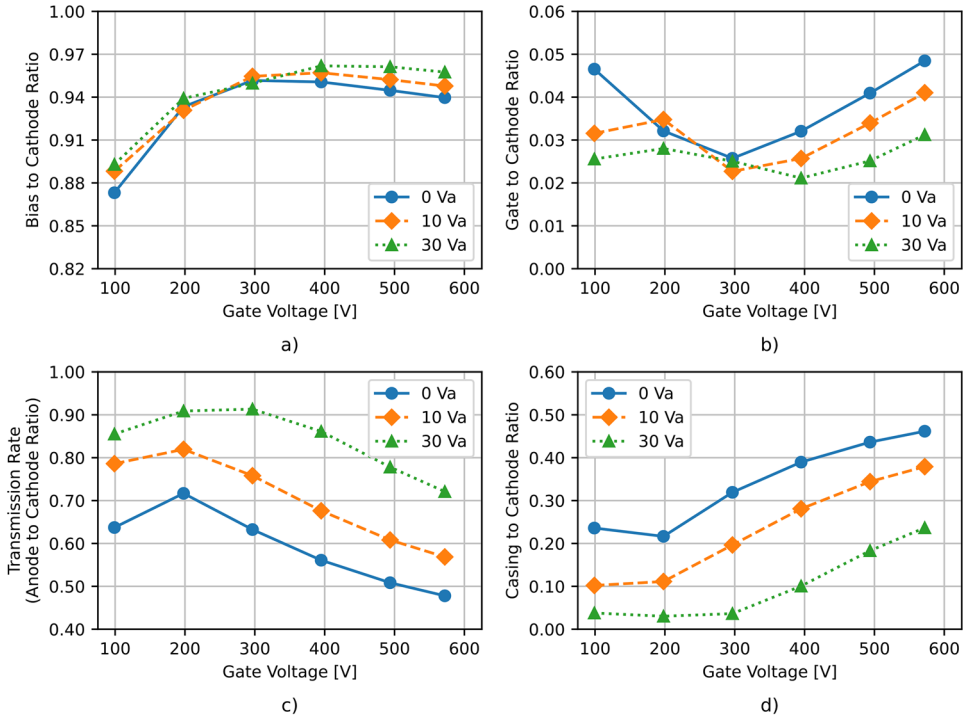

Fig. 8 Ratio between collected currents and cathode currents as a function of the gate and anode voltage; **a**) bias to cathode ratio, **b**) gate to cathode ratio, **c**) transmission rate, (anode to cathode ratio), **d**) casing to cathode ratio

100 V gate condition, in which the current lost on the focusing electrode is significant with respect to the cathode current. The performances increase with the anode voltage as the gate current is reduced. A peak condition is reached at around 300–400 V on the gate, depending on the anode voltage, where the bias to cathode ratio appears to be maximum while the gate to cathode is minimized. At low gate voltages, the weak electric field is insufficient to efficiently focus the electron beam. On the other hand, at high gate voltages, the electron density in the beam becomes too high, resulting in increased Coulomb repulsion, which broadens the beam and increases gate losses. The transmission varies with both the gate voltage and the anode voltage, reaching a maximum of 91% at 300 V on the gate and 30 V on the anode. Higher gate voltages reduce transmission by directing more current to the casing, whereas higher anode voltages increase the electrons collected by the anode by reducing the amount collected by the casing. Respect to the FEEP NU in Table 1, at 200 V of bias, the DN3.4 has a transmission rate between 70 and 90%. At higher gate voltage, the transmittance decreases to approximately 50–70% of the total cathode current as the casing current component increases.

Emitter temperature influence

Figure 9 shows the effects of the emitter temperature on the currents at 580 V on the gate and 30 V on the anode. The results for the cathode, gate, bias, anode, and casing currents are presented along with error bars showing the standard deviation of the data. The cathode current shows good repeatability and the limited temperature influence on the current confirms the space-charge limited regime in this temperature range. The current reduction at temperatures lower than 1130 °C could be explained by the emitter poisoning as the residual gasses present in the vicinity of the emitter lead to an effective

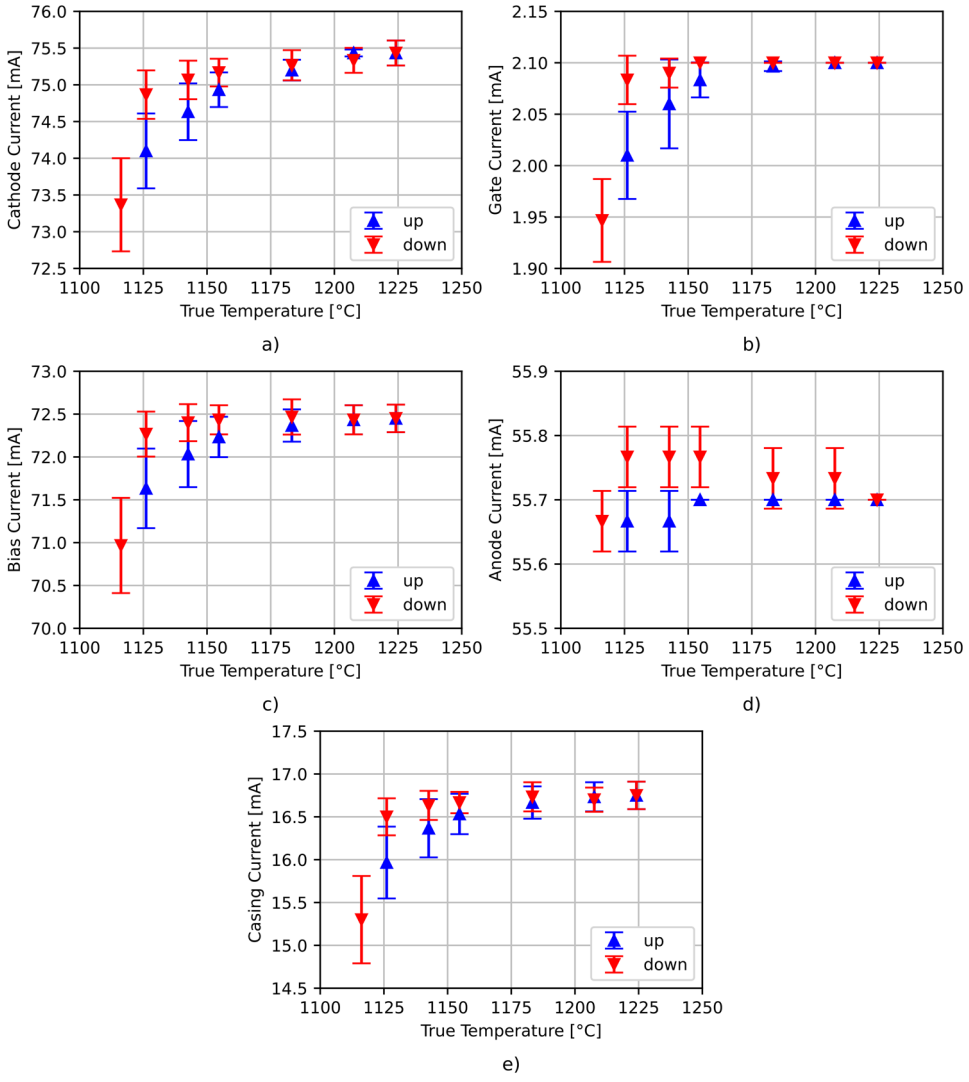

Fig. 9 Currents as a function of the cathode temperature during decreasing and increasing power; **a**) cathode current, **b**) gate current, **c**) bias current, **d**) anode current, **e**) casing current

increase of the work function [53]. A clear drop in performance is observed when reducing the cathode temperature to 1115 °C and, to avoid any damage to the emitter surface due to poisoning, the temperature was not further reduced. The emission is completely recovered once the emitter temperature is increased above 1180 °C, however at lower temperatures, a hysteresis effect occurs due to the poisoning. Poisoning recovery is possible even at these lower temperatures, but longer emission time is required to clean off the emitting surface [54]. The decrease in cathode current primarily leads to a reduction in bias current, while the gate current decreases by no more than 0.2 mA. This drop in bias current results in a reduction of casing current, while the anode current remains unchanged during the thermal sweep while the anode current remains unchanged during the thermal sweep. The stability of the anode current can be attributed to the optics configuration, as the extracted current is determined by the applied potential. Lower emission reduces the electrons diverted to the casing, minimizing space charge effects.

Operation at lower temperatures without poisoning effects is expected to be feasible at pressures lower than those present during the tests, as reported in Table 2 [51]. This

lower operating temperature would enhance the predicted emitter lifetime by reducing barium depletion and decreasing the risk of heater failure [48, 55]. Achieving lower pressures, however, was not possible under the defined operating conditions, respectively 580 V and 30 V for gate and anode. The chamber pressure was observed to rise during the operation due to anode outgassing caused by electron beam heating and electron sputtering, as confirmed by the peaks observed in the partial pressure readings shown in Table 2. It should be noted that the pressures reported in Table 2, measured at the chamber wall by the RGA, likely underestimate the actual partial pressures in the immediate vicinity of the emitter. This is due to the local outgassing of the anode and electrodes under electron bombardment, which could not be fully mitigated as only the emitter was outgassed through the heater. Consequently, local emitter poisoning effects may occur at pressures lower than what would be inferred from the RGA readings alone.

Conclusions

The DN3.4 is a propellantless neutralizer that has been designed and characterized in an experimental testing campaign at different operational parameters. The neutralizer consists of an electron gun configuration in which the emitted cathode current is extracted by a biased gate electrode and focused by a focusing electrode. The testing campaign has demonstrated that the DN3.4 is able to extract a stable current, and that the technology is suitable for delivering sufficient current for neutralizing small/CubeSat thrusters, such as the RIT3.5. With a heater power input of 10.5 W required to keep the emitter temperature stable at 1200 °C, and a gate extraction voltage of 580 V, the device is able to generate 55.8 mA of anode current, with a power-to-current ratio of 0.32 W/mA. Thus, achieving a higher emission current with an enhanced power efficiency than has been previously achieved for such applications.

The characterization demonstrated that the results are highly repeatable, and it is strongly influenced by the electrodes' optics. The gate biasing voltage is the main factor affecting the emission, while the focusing electrode reduces the current collected by the gate, increasing the efficiency of the emission. As expected, the anode voltage influences the amount of current collected by reducing the current diverging into the casing because of the electron beam self-repulsion. Moreover, initial investigations on the emitter temperature's influence on the emission suggest that the DN3.4 require a temperature in the range of 1160–1200 °C to operate without poisoning effects at 8×10^{-8} mbar of pressure. Maintaining such high temperatures results in increased power consumption and may accelerate cathode degradation, thereby reducing the overall operational lifetime of the device, highlighting the need for optimizing temperature management in future designs.

While these findings are promising, these results were obtained in diode configuration and therefore they should be validated through a coupled test with a thruster to confirm the assumptions made when recreating operational conditions with the cathode bias, and to verify that the anode effectively simulates the ion beam. Future work will address these limitations by examining poisoning phenomena at lower operating temperatures, assessing sputtering and degradation under realistic ion bombardment conditions, and conducting integrated testing with ion thrusters to better understand neutralization mechanisms and their interactions.

Author contributions
K.G. contributed to project conception, experimental system development, test preparation, data analysis, manuscript writing, and editing. Z.N. contributed to experimental system development, test preparation, data collection, and analysis. A.D.I. contributed to the project conception, experimental system development, manuscript review, and editing. F.G. and S.B.G. contributed to the project conception and design, supervised the work, and advised on the test campaign. All authors reviewed the manuscript and approved the version to be published.

Funding
This work has been conducted under the European Space Agency contract No. 4000139444/22/NL/SD and 4000134611/21/NL/MG.

Data availability
No datasets were generated or analysed during the current study.

Code availability
Not applicable.

Declarations

Competing interests
The authors declare no competing interests.

Received: 26 January 2025 / Accepted: 21 October 2025
Published online: 14 November 2025

References

1. Levchenko I, Bazaka K, Ding Y, Raitses Y, Mazouffre S, Henning T, Klar PJ, Shinohara S, Schein J, Garrigues L, Kim M, Lev D, Taccogna F, Boswell RW, Charles C, Koizumi H, Shen Y, Scharlemann C, Keidar M, Xu S (2018) Space micropropulsion systems for cubesats and small satellites: from proximate targets to furthermost frontiers. Appl Phys Reviews 5:011104. https://doi.org/10.1063/1.5007734
2. Lev D, Myers RM, Lemmer KM, Kolbeck J, Koizumi H, Polzin K (2019) The technological and commercial expansion of electric propulsion. Acta Astronaut 159:213–227. https://doi.org/10.1016/j.actaastro.2019.03.058
3. Massotti L, Siemes C, March G, Haagmans R, Silvestrin P (2021) Next generation gravity mission elements of the mass change and geoscience international constellation: from orbit selection to instrument and mission design. Remote Sens 13:3935. https://doi.org/10.3390/rs13193935
4. Dionisio S, Anselmi A, Bonino L, Cesare S, Massotti L, Silvestrin P (2018) The Next Generation Gravity Mission: challenges and consolidation of the system concepts and technological innovations. In: The 15th International Conference on Space Operations. https://doi.org/10.2514/6.2018-2495, Marseille, France
5. Walker R, Binns D, Bramanti C, Casasco M, Concari P, Izzo D, Feili D, Fernandez P, Fernandez JG, Hager P, Koschny D, Pesquita V, Wallace N, Carnelli I, Khan M, Scoubeau M, Taubert D (2018) Deep-space cubesats: thinking inside the box. Astron Geophys 59:524–530. https://doi.org/10.1093/astrogeo/aty232
6. Feili D, Smirnova M, Dobkevicius M, Di Cara DM, Massotti L, Bosch Borras E, Mingo A, Lotz B, Collingwood C (2015) Design, construction and testing of a radio frequency mini ion engine according to the propulsion requirements of the next Generation Gravity Missions NGGM. In: The Joint Conference of The 30th International Symposium on Space Technology and Science, The 34th International Electric Propulsion Conference and The 6th Nano-satellite Symposium. IEPC-2015-277/ISTS-2015-b-277, Kobe-Hyogo, Japan
7. Smirnova M, Mingo A, Schein J, Smirnov P, Bosch E, Massotti L (2019) Test Campaign on the novel variable ISP Radio frequency mini ion engine. In: The 36th International Electric Propulsion Conference. IEPC-2019-A-574, Vienna, Austria
8. Guarducci F, Lewis R, Daykin-Iliopoulos A, Marangone D, Clark S (2024) Development and industrialization of miniature radiofrequency ion thruster (RIT3.5) and neutralizer technologies for precision control satellite applications. In: The 38th International Electric Propulsion Conference. IEPC-2024-813, Toulouse, France
9. Samples SA, Wirz RE (2019) Development status of the miniature xenon ion thruster. In: The 36th International Electric Propulsion Conference. IEPC-2019-143, Vienna, Austria
10. Conversano RW, Wirz RE (2013) Mission capability assessment of cubesats using a miniature ion thruster. J Spacecr Rockets 50:1035–1046. https://doi.org/10.2514/1.A32435
11. Guarducci F, Marangone D, Clark S, Lewis R, Gabriel SB, Smirnova M, Mingo A (2022) Development and industrialization of the RIT 3.5. In: The 37th International Electric Propulsion Conference. IEPC-2022-272, Cambridge, MA, USA
12. Lev DR, Mikellides IG, Pedrini D, Goebel DM, Jorns BA, McDonald MS (2019) Recent progress in research and development of Hollow cathodes for electric propulsion. Reviews Mod Plasma Phys 3:1–89. https://doi.org/10.1007/s41614-019-0026-0
13. Gasa K, Daykin-Iliopoulos A, Bosi F, Guarducci F, Rogers E, Gabriel SB (2022) Development of a low current dry neutralizer in a Pierce gun configuration. In: The 37th International Electric Propulsion Conference. IEPC-2022-134, Cambridge, MA, USA
14. Domonkos M, Gallimore A, Williams G Jr., Patterson M (1999) Low-current hollow cathode evaluation. In: The 35th Joint Propulsion Conference and Exhibit. Los Angeles, CA, USA. https://doi.org/10.2514/6.1999-2575, Los Angeles, CA, USA
15. Wirz R, Goebel D, Marrese C, Mueller J (2003) Development of cathode technologies for a miniature ion thruster. In: The 39th AIAA/ASME/SAE/ASEE Joint Propulsion Conference and Exhibit. Huntsville, AL, USA. https://doi.org/10.2514/6.2003-4722.
16. Goebel DM, Becatti G, Mikellides IG, Lopez Ortega A (2021) Plasma Hollow cathodes. J Appl Phys 130:050902. https://doi.org/10.1063/5.0051228

17. Koshelev NN, Loyan AV (2007) Investigation of hollow cathode for low power hall effect thruster. In: The 30th International Electric Propulsion Conference. IEPC-2007-103, Florence, Italy
18. Puchkov PM (2017) The low-current cathode for a small power electric propulsion. In: EUCASS. https://doi.org/10.13009/EUCASS2017-138, Milan, Italy, p 11 pages
19. Lev D, Alon G, Appel L (2019) Low current heaterless Hollow cathode neutralizer for plasma propulsion-Development overview. Rev Sci Instrum 90:113303. https://doi.org/10.1063/1.5097599
20. Pedrini D, Ducci C, Misuri T, Paganucci F, Andrenucci M (2018) Sitael Hollow cathodes for Low-Power hall effect thrusters. IEEE Trans Plasma Sci 46:296–303. https://doi.org/10.1109/TPS.2017.2778317
21. Bock D, Drobny C, Laufer P, Kössling M, Tajmar M (2016) Development and Testing of Electric Propulsion Systems at TU Dresden. In: The 52nd AIAA/SAE/ASEE Joint Propulsion Conference. https://doi.org/10.2514/6.2016-4848, Salt Lake City, UT, USA
22. McDonald MS, Caruso NRS (2017) Ignition and early operating characteristics of a lowcurrent C12A7 hollow cathode. In: The 35th International Electric Propulsion Conference. IEPC-2017-253 /ISTS-2017-b-253, Atlanta, GA, USA
23. Gasdaska C, Falkos P, Robin M, Hruby V, Demmons N, McCormick R (2004) Testing of carbon nanotube field emission cathodes. In: The 40th AIAA/ASME/SAE/ASEE Joint Propulsion Conference and Exhibit. Fort Lauderdale, FL, USA. https://doi.org/10.2514/6.2004-3427.
24. Bock D, Tajmar M (2018) Highly miniaturized FEEP propulsion system (NanoFEEP) for attitude and orbit control of cubesats. Acta Astronaut 144:422–428. https://doi.org/10.1016/j.actaastro.2018.01.012
25. Yamamoto N, Morita T, Ohkawa Y, Nakano M, Funaki I (2019) Ion thruster operation with carbon nanotube field emission cathode. J Propul Power 35:490–493. https://doi.org/10.2514/1.B37214
26. Dankongkakul B, Wirz RE (2018) Axial Ring-Cusp hybrid (ARCH) plasma discharge: an approach to highly efficient miniature-scale ion sources. Plasma Sources Sci Technol 27:125001. https://doi.org/10.1088/1361-6595/aae63c
27. Marrese-Reading C, Polk J, Mueller J, Owens A, Tajmar M, Spindt CA, Fink R (2001) In-FEEP thruster ion beam neutralization with thermionic and field emission cathodes. In: The 27th International Electric Propulsion Conference. IEPC-01-290, Pasadena, CA, USA
28. Tajmar M (2002) Survey on FEEP Neutraliser Options. In: The 38th AIAA/ASME/SAE/ASEE Joint Propulsion Conference & Exhibit. Indianapolis, IN, USA. https://doi.org/10.2514/6.2002-4243.
29. Capacci M, Matticari G, Materassi M, Nicolini D, Frigot P-E (2009) Neutraliser for FEEPs: review on the development status. In: The 31st International Electric Propulsion Conference. IEPC-2009-013, Ann Arbor, MI, USA
30. Nicolini D (2009) LISA pathfinder field emission thruster system development program. The 60th international astronautical Congress. IAC-09.C4.1.6. Daejeon, Korea
31. Seifert B, Reissner A, Buldrini N, Krejci D, Plesescu F, Hörbe T, Scharlemann C (2014) Integrated electric propulsion systems for small satellites. In: The 4th Space Propulsion Conference. Cologne, Germany
32. Kreiji D, Reissner A, Schönherr T, Seifert B, Saleem Z, Alejos R (2019) Recent flight data from IFM nano thrusters in a low earth orbit. In: The 36th International Electric Propulsion Conference. IEPC-2019-A724, Vienna, Austria
33. Gilmour AS (2011) Klystrons, traveling wave tubes, magnetrons, crossed-field amplifiers, and gyrotrons. Artech House, Boston, MA
34. Humphries SJ (1990) Charged particle beams. John Wiley and Sons
35. Vaughan JRM (1981) Synthesis of the Pierce gun. IEEE Trans Electron Devices 28:37–41. https://doi.org/10.1109/T-ED.1981.20279
36. Gasa K, Daykin-Iliopoulos A, Guarducci F, Gabriel SB (2024) Two-dimensional modelling of a low current electron gun dry neutraliser for ion engines. In: The 38th International Electric Propulsion Conference. IEPC-2024-404, Toulouse, France
37. Gasa K, Daykin-Iliopoulos A, Guarducci F, Gabriel SB (2025) Plasma potential measurements in a dry neutraliser coupled with a RF ion thruster. In: The 39th International Electric Propulsion Conference. IEPC-2025-542, London, United Kingdom
38. Daykin-Iliopoulos A, Gasa K, Lewis R, Marangone D, Clover J, Clark S, Guarducci F, Gabriel SB, Smirnova M, Kigonya J, Rizzieri Daniele, Feili D, Guevara Jelid HI, Wallace N (2025) Radio frequency ion engine and dry neutralizer development and coupled testing for CubeSat missions. In: The 39th International Electric Propulsion Conference. IEPC-2025-583, London, United Kingdom
39. Loyan AV, Titov M, Rybalov O, Maksymenko T (2013) Middle power hall effect thrusters with centrally located cathode. In: The 33rd International Electric Propulsion Conference. IEPC-2013-410, Washington, D.C., USA
40. Lev DR, Alon G (2018) Operation of a Hollow cathode neutralizer for Sub-100-W hall and ion thrusters. IEEE Trans Plasma Sci 46:311–318. https://doi.org/10.1109/TPS.2017.2779409
41. Ziemer J, Gamero-Castaño M, Hruby V, Spence D, Demmons N, McCormick R, Roy T, Gasdaska C, Young J, Connolly B (2005) Colloid micro-newton thruster development for the ST7-DRS and LISA Missions. In: The 41st AIAA/ASME/SAE/ASEE Joint Propulsion Conference & Exhibit. https://doi.org/10.2514/6.2005-4265, Tucson, AZ, USA
42. Laufer P, Tajmar M (2019) CNT-based cold electron source for space applications on nanosatellites. In: The 36th International Electric Propulsion Conference. IEPC-2019-477, Vienna, Austria
43. Capacci M, Materassi M, Noci G (2007) Development and qualification of a neutralizer device for the FEEP Micro Propulsion on Microscope and Lisa Path Finder. In: The 30th International Electric Propulsion Conference. IEPC-2007-154, Florence, Italy
44. Grimaud L, Kreiji D, Seifert B (2019) The IFM Micro FEEP thruster: a modular design for smallsat propulsion. In: The 36th International Electric Propulsion Conference. IEPC-2019-A675, Vienna, Austria
45. Krejci D, Hugonnaud V, Schönherr T, Little B, Reissner A, Seifert B, Koch Q Borràs EB Full performance mapping of the IFM nano thruster, including direct thrust measurements. J Small Satellites 8:881–893
46. Goebel DM, Katz I (2008) Fundamentals of electric propulsion: Ion and Hall Thrusters, 1st Edition. J. Wiley& Sons
47. Gaertner G, Knapp W, Forbes RG (2020) Modern developments in vacuum electron sources. Springer International Publishing
48. Cronin JL (1981) Modern dispenser cathodes. IEE Proc I Solid State Electron Devices UK 128:19. https://doi.org/10.1049/ip-i-1.1981.0012
49. Daykin-Iliopoulos A, Golosnoy IO, Gabriel SB, Bosi F (2019) Characterisation of a 30 a heaterless hollow cathode. In: The 36th International Electric Propulsion Conference. IEPC-2019-802, Vienna, Austria
50. Cronin JL (1979) Practical aspects of modern dispenser cathodes. Microw J 15:150–183

51. Bieniosek FM, Henestroza E, Houck T, Kwan JW, Leitner M, Miram G, Prichard B, Roy PK, Waldron W, Westenskow G, Yu S (2009) DARHT 2 kA cathode development. University of California, Berkeley, California
52. Akimov PV, Schamel H, Kolinsky H, Ender AYa, Kuznetsov VI (2001) The true nature of space-charge-limited currents in electron vacuum diodes: A lagrangian revision with corrections. Phys Plasmas 8:3788–3798. https://doi.org/10.1063/1.1383287
53. Jenkins RO, Trodden WG (1959) The poisoning of impregnated cathodes. J Electron Control 7:393–415. https://doi.org/10.1080/00207215908937223
54. Spectra-Mat (2014) Inc. Guidelines for Processing of Dispenser Cathodes
55. Brodie I, Jenkins RO, Trodden WG (1959) Evaporation of barium from cathodes impregnated with barium–Calcium–Aluminate. J Electron Control 6:149–161. https://doi.org/10.1080/00207215908937137

Publisher's note